

# PCCP

Accepted Manuscript



This is an *Accepted Manuscript*, which has been through the Royal Society of Chemistry peer review process and has been accepted for publication.

*Accepted Manuscripts* are published online shortly after acceptance, before technical editing, formatting and proof reading. Using this free service, authors can make their results available to the community, in citable form, before we publish the edited article. We will replace this *Accepted Manuscript* with the edited and formatted *Advance Article* as soon as it is available.

You can find more information about *Accepted Manuscripts* in the [Information for Authors](#).

Please note that technical editing may introduce minor changes to the text and/or graphics, which may alter content. The journal's standard [Terms & Conditions](#) and the [Ethical guidelines](#) still apply. In no event shall the Royal Society of Chemistry be held responsible for any errors or omissions in this *Accepted Manuscript* or any consequences arising from the use of any information it contains.



Journal Name

ARTICLE

## When do defectless alkanethiol SAMs in ionic liquids become penetrable? A molecular dynamics study

Sergey A. Kislenco,<sup>a,\*</sup> Victoria A. Nikitina<sup>b</sup> and Renat R. Nazmutdinov<sup>c,\*</sup>Received 00th January 20xx,  
Accepted 00th January 20xx

DOI: 10.1039/x0xx00000x

www.rsc.org/

Molecular dynamics simulations were performed to address the permeability of defectless alkanethiol self-assembled monolayers (SAMs) on charged and uncharged Au(111) surfaces in 1-butyl-3-methylimidazolium ([bmim][BF<sub>4</sub>]) room-temperature ionic liquid (IL). We demonstrate that ionic permeation into the monolayer does not start until a critical surface charge density value is attained (both for positive and negative surface charges). The free energy barrier for the permeation of IL components is shown to include nearly equal contributions from the ion desolvation and the channel formation in the dense monolayer. Long chain alkanethiols (hexadecanethiol SC<sub>16</sub>H<sub>33</sub>) exhibit superior barrier properties as compared with short chain alkanethiols (hexanethiol SC<sub>6</sub>H<sub>13</sub>) due to the dense packing of alkanethiol chains in highly ordered zigzag conformation oriented at the same tilt angle. Computed critical charge densities correspond to the electrode potential values beyond the limits of the monolayer stability which might indicate the defectless monolayer impermeability towards the IL components. Experimental findings on increased interfacial capacitance are interpreted, therefore as some manifestation of the monolayer defectiveness occurring in real electrochemical systems. The potential of mean force is constructed for a typical redox probe ferrocene/ferrocenium (Fc/Fc<sup>+</sup>) as well, to investigate a possible permeation of the solute from the IL into the SC<sub>6</sub>H<sub>13</sub> monolayer.

### 1. Introduction

Alkanethiol SAMs are widely employed both in fundamental electrochemical kinetic studies<sup>1-4</sup> and various practical applications, such as bioelectrochemical sensors, surface patterning, material functionalisation.<sup>5,6</sup> That is why any possibility to control the monolayer permeability towards the solution components is of major importance.

The permeability of the monolayers towards redox-active species present in solutions can be tested in kinetic electrochemical experiments, when the electrode-reactant separation is controlled via Au surface modification with alkanethiols with different chain lengths. This experimental arrangement provides a very precise (though indirect) test of the influence of various defects on the electron transfer (ET) rate in the diabatic (weak coupling) regime.<sup>7</sup> The exponential dependence of the apparent rate constant on the monolayer thickness is often regarded as a characteristic feature of a defectless monolayer, impermeable towards reactant species.

Alkanethiol monolayers on gold in aqueous solutions were found to be impermeable towards Fe(CN)<sub>6</sub><sup>3-/4-</sup>, [Ru(NH<sub>3</sub>)<sub>6</sub>]<sup>3+</sup> and other common reactants.<sup>8,1-4</sup> However, at relatively small electrode-reactant separations (typically less than 6 ÷ 8 Å) the ET rate constant becomes distance independent, as the reaction proceeds under adiabatic (strong coupling) control. In this case kinetic measurements cannot provide information regarding the permeability of alkanethiol monolayers with relatively short chains (SC<sub>n</sub>H<sub>2n+1</sub>, n ~ 1 ÷ 6).

Impedance spectroscopy and cyclic voltammetry are typically applied to study ionic permeability of SAMs contacting with electrolyte solutions when no redox active probes are present. Most of data available on the permeability of monolayers is related to aqueous solutions, as alkanethiol monolayers were found to be unstable in most of the organic solvents. It was found that the insulating properties of alkanethiol monolayers towards different ions differ greatly.<sup>8,9</sup> For instance, alkanethiol monolayers with relatively short chains (SC<sub>n</sub>H<sub>2n+1</sub>, n < 10) are permeable for Cl<sup>-</sup> and ClO<sub>4</sub><sup>-</sup> ions, while no permeation is observed for highly hydrated F<sup>-</sup> ion.<sup>8</sup> This finding illustrates the major role of solvent-ion interaction in the process of ionic permeation into the monolayer.

The permeability of alkanethiol monolayers is generally dependent on the monolayer thickness<sup>8,10,11</sup> and electrode potential.<sup>12,10,13,14</sup> One possible reason for the permeability of alkanethiol SAMs is their defectiveness, as channels for the ions to penetrate the monolayer are formed at defective sites. Van der Waals stabilizing interactions between alkyl chains of shorter thiols are weaker than those for longer alkanethiols

<sup>a</sup> Joint Institute for High Temperatures of RAS, Izhorskaya 13/19, 125412, Moscow, Russian Federation. E-mail: kislenco@ihed.ras.ru

<sup>b</sup> M. V. Lomonosov Moscow State University, Leninskie Gory 1/3, 199991, Moscow, Russian Federation.

<sup>c</sup> Kazan National Research Technological University, 420015, K. Marx Str. 68 Kazan, Russian Federation. E-mail: nazmutdi@mail.ru

† Electronic Supplementary Information (ESI) available: Snapshot of the simulation box; dihedral angle distributions in monolayers; qualitative surface charge induced changes of the potential of mean force for anion [BF<sub>4</sub>]<sup>-</sup>; on the question of the permeability of real alkanethiol SAMs; changes in the SC<sub>16</sub>H<sub>33</sub> monolayer structure after the permeation of ions. See DOI: 10.1039/x0xx00000x

and thus more defects inside the monolayer exist, which results in the enhanced permeability of SAMs. The authors of refs 10, 12 state that ionic permeation does not start until a critical cathodic potential value is exceeded, as it induces structural changes in the monolayer leading to defect formation.

However, an alternative treatment of the ionic permeation phenomena has been recently reported.<sup>15,16</sup> The existence of an activation energy barrier is postulated for ions at a monolayer/electrolyte interface. The magnitude of this barrier is determined by the size of a pinhole defect inside the monolayer and by the electric field across the interface. This concept can explain the existence of the critical potential for ionic permeation, although it still requires assuming the presence of defects in the monolayer.

The permeation of the electrolyte ions inside the defectless close-packed monolayer is also considered to be possible. The existence of 3 Å channels in the monolayer is suggested in ref 9. Such channels enable the transport of small ions and solvent molecules into the monolayer in the absence of pinholes and other types of packing defects. These findings are indirectly supported by experimental observations: capacitance vs. scan rate and phase angle vs. frequency dependencies, AFM and STM spectroscopic studies on the formation of uniform UPD layers of various metals at alkanethiol-coated substrates.

In refs 13, 17 the conformation of alkanethiol group is assumed to change when the threshold potential value is exceeded, allowing ions to penetrate the restructured monolayers. In this scenario the monolayers are permeable towards ions and small solvent molecules regardless of the presence or formation of defects in the course of penetration. In the anodic limit the critical potential for ionic permeation was found as well.<sup>14</sup> Structural changes of the monolayer were attributed to the effect of permeating ions.

So far the data on the permeability of alkanethiol SAMs in non-aqueous solvents and room-temperature ionic liquids (ILs) are very scarce. This hinders quantitative interpretation of kinetic information on the ET through barrier layers in these solvents.<sup>18,19</sup> Studies of molecular permeability of thiol adlayers in ionic liquids are also of crucial importance for molecular recognition in IL sensing applications.<sup>20</sup>

In our previous experimental study alkanethiol SAMs on gold were found to exhibit high permeability towards the ions of 1-butyl-3-methylimidazolium tetrafluoroborate ([bmim][BF<sub>4</sub>]) and 1-n-hexyl-3-methylimidazolium tris(pentafluoroethyl)trifluorophosphate ILs.<sup>11</sup> Anomalously high capacitance values were observed even for undecanethiol adlayers, which are stable against the permeation of ions in aqueous solutions.<sup>8,21,22</sup> Surprisingly, these monolayers kept their barrier properties in respect to Fc/Fc<sup>+</sup> reaction (at least for alkanethiols with 6 – 18 methylene units in alkyl chain). These results along with prior controversies in the interpretation of kinetic and capacitance data call for further studies of molecular mechanism of ionic permeation.

Previously we explored microscopic details of the transport of electrolyte ions through alkanethiol monolayers at the Au(111)/NaF solution interface using the classical molecular

dynamics method.<sup>23</sup> The results point to the important role of water molecules when forming channels in the monolayer. In this work we extend this approach to the Au(111)/SAM/[bmim][BF<sub>4</sub>] interface. The alkanethiol SAM had a defectless close-packed ( $\sqrt{3} \times \sqrt{3}$ )R30° structure. The monolayer permeability is modeled as a function of the electrode charge and for alkanethiols with different chain length. A Fc<sup>+</sup>/Fc redox couple at the SAM/[bmim][BF<sub>4</sub>] interface is investigated as well, in order to provide interpretation for previous kinetic studies. To the best of our knowledge no attempts were made so far to address ionic transport across such electrochemical interfaces at an atomistic level.

This paper is organized as follows. Pertinent details of the MD simulations are reported in Section 2. The most important results are discussed in Section 3. Concluding remarks can be found in Section 4.

## 2. Computational details

We focused on the permeability investigation of the hexanethiol SC<sub>6</sub>H<sub>13</sub> and hexadecanethiol SC<sub>16</sub>H<sub>33</sub> monolayers. To simulate the Au(111)/SAM/[bmim][BF<sub>4</sub>] interface we used the simulation box shown in Fig. S1 (ESI<sup>†</sup>). This box represents two parallel Au(111) single-crystal surfaces 43.95×35.53 Å<sup>2</sup> in area and 7.2 Å in width, arranged at a distance of 65.6 Å and 76.1 Å for the case of SC<sub>6</sub>H<sub>13</sub> and SC<sub>16</sub>H<sub>33</sub>, respectively. One of the Au(111) surfaces was covered by the defectless ( $\sqrt{3} \times \sqrt{3}$ )R30° alkanethiolate lattice.<sup>24</sup> The gap between the surfaces was filled with the solvent. The number of [bmim][BF<sub>4</sub>] ion pairs in the solvent region was 256. A slab of the electrolyte with two free surfaces was constructed first and pre-equilibrated during 0.5 ns. Then, the adjacent Au(111) surfaces (one of which was covered by the thiol monolayer) were placed to the free surfaces of the electrolyte. Then the distance between the metal slabs was reduced with a variable step from 0.5 to 1 Å until the electrolyte density far from electrode surfaces took a value of 1.15 g·cm<sup>-3</sup> (obtained by NPT simulations of bulk electrolyte at 350 K and 1 atm.). 3D periodic boundary conditions were employed. To reduce the interaction between the simulation box and its images the periodicity in the direction perpendicular to the surfaces was elongated to 25 nm.

The MD simulations were performed for the uncharged Au(111) surfaces as well as for the charged ones. To imitate the surface charge, we applied an external electric field  $E$  directed perpendicular to the gold surfaces and related to the surface charge density  $\sigma$  of the oppositely charged surfaces through the equation  $E = 4\pi\sigma$ . All charge densities in the next section correspond to the alkanethiol-modified gold. In the present work we did not take into account the electronic polarization of the alkanethiol monolayer which presumes the dielectric constant value of 1, while the real dielectric constant of thiol adlayer is close to 2.<sup>25</sup> This was taken into account as an effective increase of the electrode charge density for a given  $E$  value. To avoid numerical errors caused by the interaction of the system (polarized under the external field)

with its periodic images in the field direction, we employed the modified 3D Ewald summation for the calculation of electrostatic interactions.<sup>26</sup> A real space cutoff of 1.5 nm was used to calculate the electrostatic interaction.

The Lopes force fields was used for [bmim][BF<sub>4</sub>] and the Fc molecule.<sup>27,28</sup> The force field parameters for Fc<sup>+</sup> were derived by ourselves in our previous work.<sup>29</sup> By analogy with the Fc model, Fc<sup>+</sup> was treated as a rigid molecule with only one internal degree of freedom – rotation of cyclopentadienyl rings around their centroid. The geometry of the Fc<sup>+</sup> molecule was obtained on the basis of DFT (B3LYP) calculations. The partial atomic charges were calculated with the help of the CHELPG method and Boltzmann averaging over eclipsed and staggered equilibrium conformations. The van der Waals interactions are addressed using the work by Lopes et al.<sup>28</sup>

Since the force fields mentioned above are based on the OPLS-AA force field, we used the original OPLS-AA parameters for thiol molecules. The Au–S bond stretching and Au–S–CT angle bending parameters as well as Lennard-Jones parameters for Au atoms were adopted from the work by Rai et al.<sup>30</sup>

The MD simulations were performed in the NVT ensemble at T = 350 K kept constant using the Nose–Hoover thermostat. The motion equations were solved using the Verlet leapfrog integration algorithm with a time step of 1 fs. The cutoff radius of the van der Waals interaction was 1.5 nm. Two simulations starting from different initial configurations were performed in order to reduce a statistical error. The interface structure was obtained by averaging over two configurations and over 4 ns of dynamics per configuration. All starting configurations were equilibrated during 1.5 ns of simulation at 350 K before collecting data.

Potential of mean force profiles (PMF) for Fc and Fc<sup>+</sup> and IL ions in [bmim][BF<sub>4</sub>] as a function of distance to the Au(111) surface modified by SAM were calculated according to procedure thoroughly described in our previous work.<sup>29</sup> To insert the Fc molecule in the ionic liquid we removed first a [BMIM][BF<sub>4</sub>] ion pair to create a cavity inside the IL at a given distance from the metal surface; the Fc molecule was placed in this cavity at the next step. Dealing with Fc<sup>+</sup> we replaced the [BMIM]<sup>+</sup> cation by the ferrocenium ion to keep electroneutrality.

All MD simulations were performed using the DL\_POLY package<sup>31</sup> and the supercomputers MVS-100 K (Joint Supercomputer Center of the Russian Academy of Sciences), SKIF MSU «Chebyshev» and «Lomonosov» (Moscow State University).

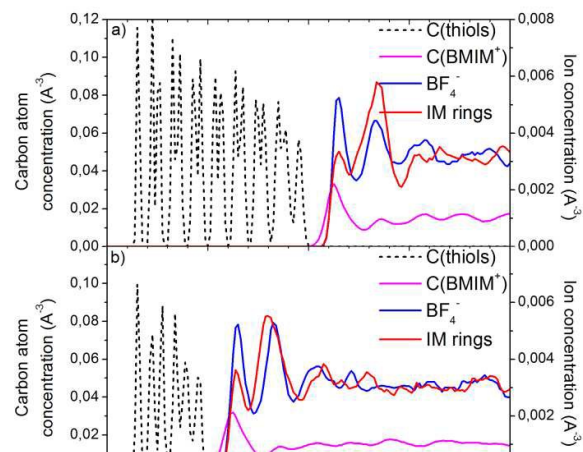


**Fig. 1** Au(111)/SC<sub>16</sub>H<sub>33</sub>/[bmim][BF<sub>4</sub>] (a) and Au(111)/SC<sub>6</sub>H<sub>13</sub>/[bmim][BF<sub>4</sub>] (b) interface structures (the surface charge is zero). Blue and red lines denote the distribution of anions and imidazolium rings, respectively. Black dotted line denotes the distribution of C atoms in the monolayer. Magenta line shows the distribution of C atoms of the [bmim]<sup>+</sup> cation.

### 3. Results and discussions

#### 3.1. Structure of the Au(111)/SAM/[BMIM][BF<sub>4</sub>] interface at the potential of zero charge

Fig. 1 shows distribution of various system components at Au(111)/SC<sub>16</sub>H<sub>33</sub>/[bmim][BF<sub>4</sub>] and Au(111)/SC<sub>6</sub>H<sub>13</sub>/[bmim][BF<sub>4</sub>] interfaces at the potentials of zero charge (Au(111) surface charge density  $\sigma = 0$ ). The IL structure is rather similar at the both interfaces. Sharp boundaries are observed between the monolayer and liquid phase, which indicate the absence of ionic permeation into the monolayer. This agrees well with the experimental findings in aqueous electrolyte solutions.<sup>10,12,13</sup> The IL components form a layered structure similar to that observed in the vicinity of solid surfaces.<sup>29,32-34</sup> However, the amplitude of ionic concentration oscillations near the IL/SAM interface is significantly lower and IL ions in the monolayer closest vicinity are thus less ordered, which is not surprising due to the softness of alkanethiol monolayers as compared with crystalline solids.

A peak in the distribution of C atoms of the [bmim]<sup>+</sup> cation is observed at  $z = 22.5$  Å in Fig. 1a and  $z = 12.5$  Å in Fig. 1b. The peak is located between the monolayer surface and the highest peak in the imidazolium ring distribution indicating that the [bmim]<sup>+</sup> cations in the vicinity of the monolayer are oriented with their alkyl chains towards the alkanethiol monolayer. This structure resembles, therefore a lipid bilayer.

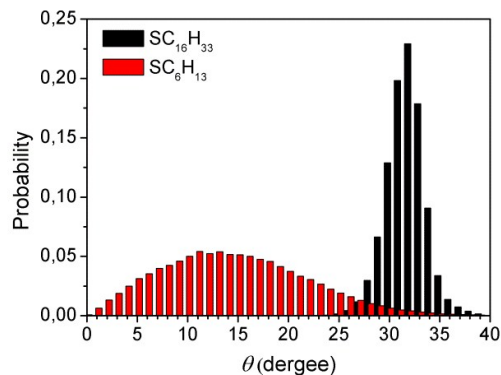


Fig. 2 Tilt angle distributions for  $SC_6H_{13}$  and  $SC_{16}H_{33}$  monolayers.

Despite the same packing density of molecules in  $SC_6H_{13}$  and  $SC_{16}H_{33}$  monolayers, the orientation of the molecules in these two monolayers is quite different. The monolayer structure is characterized by dihedral angle distributions in the alkanethiol molecules (Fig. S2, ESI<sup>†</sup>) and distributions of a tilt angle relative to the surface normal (Fig. 2). The longer alkanethiol shows close to ideal molecular arrangement: all molecules are in zigzag conformation (Fig. S2a, ESI<sup>†</sup>) with the same tilt angle (Fig. 2). The average tilt angle for  $SC_{16}H_{33}$  monolayer is close to  $30^\circ$ , which is in good agreement with experiment.<sup>24</sup> The observed highly ordered structure forms mainly due to the stabilizing of van der Waals interactions between alkyl chains of the alkanethiol molecules. Van der Waals interactions between the chains of shorter alkanethiols are too weak to make the monolayer stable enough, which leads to the increase in the monolayer disorder due to thermal motion. In this case various alkyl chain conformations in the monolayer coexist (Fig. 2b, ESI<sup>†</sup>). The tilt angle distribution is wider (Fig. 2), and the tilt angle average value is lower ( $\sim 10^\circ$ ), and thus the density of atoms in the direction perpendicular to the substrate surface is lower in a hexanethiol monolayer.

### 3.2. SAMs permeability as a function of the surface charge density

We studied the dependence of the ionic permeability of dense defectless alkanethiol monolayers on the electrode charge density  $\sigma$  (Fig. 3). The plots in Fig. 3 indicate that the permeation of ions inside the monolayer does not start until a critical charge density value is reached. It means that upon approaching this threshold charge density (or electrode potential) value the monolayer loses its barrier properties towards the IL components, i.e. the penetration of both the cations and the anions becomes feasible. Cathodic and anodic critical surface charge density values were determined via linear extrapolation of the  $n_s$  vs  $\sigma$  dependencies (Table 1). It has to be kept in mind that these results are related to a local equilibrium which is attained during several nanoseconds. A more precise functional form of these dependencies may be determined from longer simulations with the account for the permeability dependence on the number of ions, which already reside inside the monolayer and alter its structure.

One can say that the process of permeation of ions inside the monolayer is formally similar to the well-studied process of lipid bilayer electroporation, which also becomes permeable

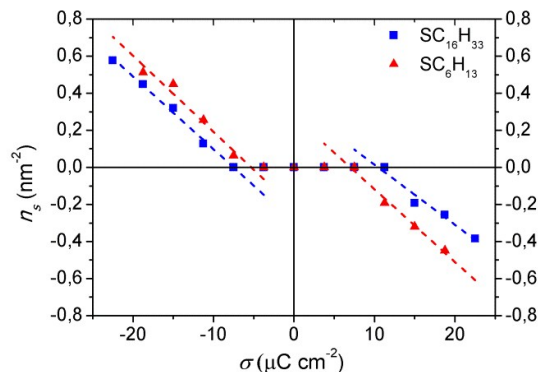
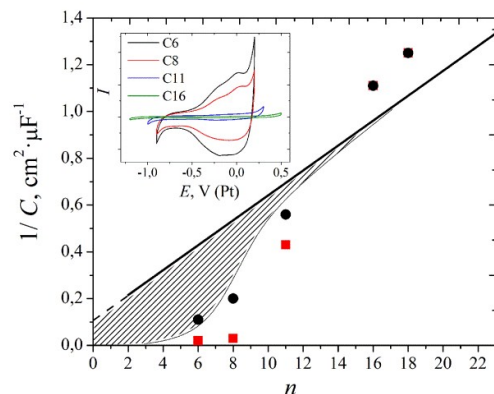


Fig. 3 The surface concentration of ions which penetrate through the monolayer,  $n_s$ , vs the electrode charge density,  $\sigma$ .

under critical electric field value (ca.  $0.1 \text{ V}\cdot\text{nm}^{-1}$ ).<sup>35,36</sup> However, the two permeation mechanisms differ significantly. After reaching a critical electric field value the hydrophilic lipid dipolar heads in the bilayer reorient forming a hydrophilic nanopore.<sup>37</sup> Nonpolar alkyl chains in the alkanethiol SAM are bound to the surface. An external electric field itself does not induce, therefore, structural changes in the monolayer, and critical  $E$  values for alkanethiol SAMs are much higher than those for the lipid bilayers (Table 1). Fig. 3 shows that the threshold charge density values for hexadecanethiol are higher as compared with those for hexanethiol. This finding agrees with the literature data for aqueous electrolyte solutions.<sup>10</sup>

We should note that the ionic permeation is a reversible process. The switching off an external electric field results in the expulsion of ions back to the IL phase and the monolayer regains its structure, which is confirmed experimentally.<sup>14</sup> The main driving force that returns ions into the liquid phase is the electrostatic attraction between ions in the monolayer and uncompensated charges of opposite sign in the ionic liquid.

Some experimental evidence in favor of the permeability of alkanethiol monolayers in  $[bmim][BF_4]$  was obtained in our previous work.<sup>11</sup> In this study we found that cyclic voltammograms of hexanethiol-, octanethiol- and undecanethiol-coated Au exhibit a pronounced asymmetry. For relatively short alkanethiols capacitance in the region of more positive potential values is much higher than that in the area of more negative potential values. This may be attributed to the manifestation of permeation of IL anions into the monolayer. Fig. 4 shows the dependence of the inverse capacitance values for  $Au/SC_nH_{2n+1}/[bmim][BF_4]$  interfaces ( $n = 6, 8, 11, 16, 18$ ) on the monolayer thickness. We plot two capacitance values for each alkanethiol: capacitance calculated from cyclic voltammograms at the formal potential of  $Fc^+/Fc$  reaction, which corresponds to the anomalous region of increased capacitance and minimal capacitance (in the "normal" region). The data for aqueous solutions are presented schematically by a thick straight line (general trend) and thin curved line (deviations for chloride solutions).<sup>8</sup> The linearity of inverse capacitance vs. chain length dependence is characteristic for impermeable monolayer. In chloride containing aqueous solutions deviations from linearity are



**Fig. 4** The plot of reciprocal capacitance  $1/C$  vs the number of methylene units in the alkanethiol monolayer  $n$  in  $[\text{bmim}][\text{BF}_4]$ . The thick line presents  $1/C$  vs  $n$  dependence for surface-inactive aqueous electrolytes, thin line marks the region of capacitances decreased in the presence of chloride, both sets of data taken from ref. 8. Capacitances at formal potential of  $\text{Fc}^+/\text{Fc}$  from cyclic voltammetry (■) and minimal capacitances from cyclic voltammograms (●) are shown. Inset: cyclic voltammograms of alkanethiol-modified Au polycrystalline electrodes.

observed (dashed region in Fig. 4). In  $[\text{bmim}][\text{BF}_4]$  these deviations are even more pronounced, which is indicative of higher permeability of alkanethiol monolayers in IL.

The shape of cyclic voltammograms of alkanethiol-modified Au electrodes is illustrated by the inset of Fig. 4. The asymmetry in the experimental cyclic voltammograms of thiol-modified gold in IL is similar to the features, observed in the cyclic voltammograms of porous carbons. Asymmetric cyclic voltammograms are observed when the sizes of cations and anions that can penetrate the pores of the material differ to a large extent, e.g. asymmetric curves are obtained with tetrabutylammonium tetrafluoroborate as a supporting electrolyte in propylene carbonate, whereas the difference in capacitance values in the region of positive and negative surface charges is not observed for tetraethyl- and tetrabutylammonium salts.<sup>38,39</sup> Similar effects can be observed in ILs at microporous carbons. The mechanism of the ionic permeation into the porous carbons and ILs is assumed to be essentially the same and the energy barrier for the permeation includes the same major contributions: desolvation, electrostatic and specific interactions of the ions with the electrode surface.

One important issue has to be taken into account which provides at least semi-quantitative comparison of the experimental and computational results. Considering that the lengths of  $\text{SC}_6\text{H}_{13}$  and  $\text{SC}_{16}\text{H}_{33}$  monolayers are approximately 1 and 2 nm (Fig. 1a and 1b), the critical electric field values (Table 1) imply enormously high electrode potentials (relative to bulk electrolyte), which can be hardly attained in a real experiment. The stability potential range for hexanethiol monolayer is ca. 1 V (Fig. 4), while the computed critical charge density values for the model defectless monolayer corresponds to the potentials ca. -3 V and +4 V vs potential of zero charge. The same is true for the hexadecanethiol monolayer. Therefore at experimental conditions *defectless* alkanethiol monolayers are assumed to be practically impermeable towards the IL ions. The monolayer permeability (i.e. decreasing the permeation energy barrier) observed

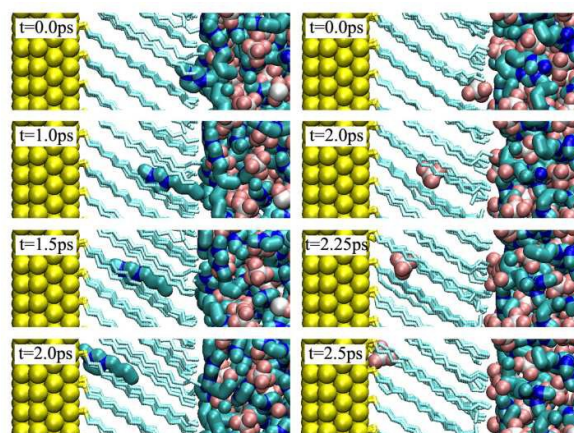


**Fig. 5** Snapshots of the elementary act of cation  $[\text{bmim}]^+$  (left side) and  $[\text{BF}_4]^-$  anion (right side) penetration into the  $\text{SC}_{16}\text{H}_{33}$  monolayer built for the electrode charge densities  $\sigma = \pm 15 \mu\text{C}\cdot\text{cm}^{-2}$ .

indirectly in experiment as the interfacial capacitance response might be attributed to the monolayer defects, which facilitate ionic transport (see more details in ES†). Again, for the model SAMs (which are still stable when the critical potential value is reached) the permeation of ions proceeds without significant structural rearrangement of the monolayer.

Cyclic voltammetry data also shows that the permeability of alkanethiols depends on their chain length, as for the longest alkanethiols the asymmetry of cyclic voltammograms disappears and capacitance values become close to the value reported for aqueous solutions (Fig. 4). This agrees with the results of our simulations, as we found different permeability for  $\text{SC}_6\text{H}_{13}$  и  $\text{SC}_{16}\text{H}_{33}$  monolayers.

In spite of a large number of investigations on the ionic permeability of alkanethiols, various interpretations of the electrochemical data have been proposed so far. In a number of works the permeability of monolayers towards solution components is attributed to the presence of defective sites in the monolayer.<sup>8,10,12,15,16</sup> Other authors maintain the possibility of ionic penetration through defectless monolayer.<sup>9,13,17</sup> Our MD study resolves somewhat these interpretation controversies, as we found that defectless alkanethiol monolayers are impermeable towards the ionic species in solution in the experimental region of electrode potentials, and some features such as increased experimental capacitance values might be explained in terms of the enhanced permeation of ions into defective monolayers. The most important, however, is to gain microscopic information on the mechanism of ionic transport through the SAM. This challenging issue is addressed in the next sub-Section.

**Table 1.** Critical charge density values  $\sigma^*$  ( $\mu\text{C}\cdot\text{cm}^{-2}$ ) and corresponding critical electric field values  $E^*$  ( $\text{V}\cdot\text{nm}^{-1}$ ).

SAM	cathodic region		anodic region	
	$\sigma^*$	$E^*$	$\sigma^*$	$E^*$
$\text{SC}_6\text{H}_{13}$	-5.3	3.0	+7	-4.0
$\text{SC}_{16}\text{H}_{33}$	-7.5	4.2	+10	-5.7

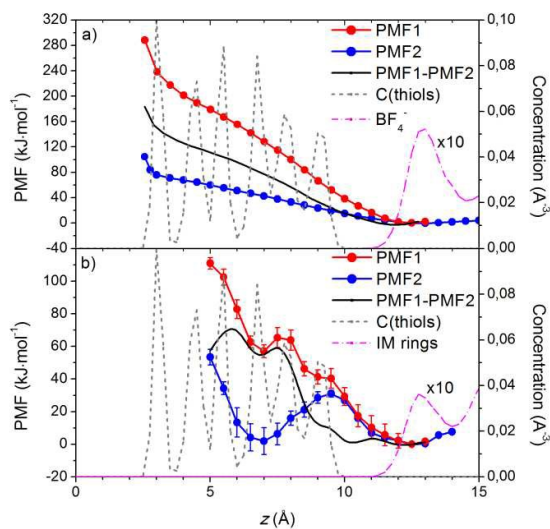


**Fig. 6** Potentials of mean force calculated for the anion  $[\text{BF}_4]^-$  (a) and cation  $[\text{BMIM}]^+$  (b) through the hexanethiol monolayer ( $\sigma = 0$ ).

### 3.3. Elementary act of ion penetration into SAMs

Earlier in ref 9 the authors discussed a possible scenario of ionic permeation into defectless alkanethiol monolayer through assumed 3 Å channels. Our results clearly show that the size of channels is overestimated. Moreover, a careful consideration of the van der Waals radii of atoms and alkanethiol tilt angle leads to the conclusion that no cavities are present in a defectless monolayer, which would provide necessary channels for ions to penetrate across the SAM.

An important feature of the mechanism of ionic permeation is that the IL ions are *dragged* into the monolayer by an external electric field. In this process alkanethiol chains are pushed away by the ions creating thus a channel for ions. Fig. 5 shows snapshots illustrating the process of the  $[\text{bmim}]^+$  cation and  $[\text{BF}_4]^-$  anion penetration into the  $\text{SC}_{16}\text{H}_{33}$  SAM on Au(111). Note that a big asymmetric cation  $[\text{bmim}]^+$  in the monolayer orients itself in a way to minimize its projection on the plane perpendicular to the ion path. Cation methyl group is always oriented towards the gold surface, and the butyl tail points away from it.

It is important to stress that the mechanism of the ion permeation into alkanethiol monolayers in ILs is quite different from that in aqueous systems, where the ions move towards the surface through polar channels formed by water molecules.<sup>23</sup> These water molecules are dragged into the non-polar monolayer due to local fluctuations of electric field at the alkanethiol/electrolyte solution interface.

A  $[\text{BF}_4]^-$  anion moves inside the monolayer through a channel formed by 3-4 alkanethiols, similar to the model proposed in ref 9, while the intrusion of a flat asymmetric  $[\text{bmim}]^+$  cation into the monolayer needs a channel containing 4-6 alkanethiol molecules. We have performed calculations of the potential of mean force (PMF) for the IL ions penetrating through the hexanethiol monolayer at the

uncharged gold surface to gain a deeper insight into the ion intrusion energetics. The red curve (PMF1) in Fig. 6a corresponds to the potential of mean force profile for  $[\text{BF}_4]^-$ . It can be seen that the PMF gradually increases with the decrease of the ion – metal surface separation. At the distance of  $z < 3$  Å the PMF slope becomes noticeably larger, which can be attributed to the van-der-Waals repulsion between the ion and the surface Au atoms.

A gradual increase in the PMF results from the energy loss due to the ion desolvation and cavity formation. To separate these contributions, we performed calculations of the PMF describing the intrusion of a single anion and a cation into the monolayer (without any other IL ions in the system, see blue line PMF2 in Fig. 6a). The difference between the red and the blue curves can be associated with the energy required to desolvate the ion. As show our calculations, the desolvation and for the channel formation energy are nearly of the same order of magnitude.

When the Au surface is charged positively, the free energy of the anion decreases. To illustrate this effect qualitatively we corrected the computed PMF profile to the contribution from the electric field ( $E=4\pi\sigma/\epsilon$ , where  $\epsilon\sim 2$ ) work (Fig. S3, ESI<sup>†</sup>). For the ion permeation to take place, the difference in the ion free energy in the bulk and at the gold surface must be comparable with  $\sim k_B T$ . This becomes possible when a critical surface charge density value  $\sigma^*$  is attained. Such a scenario supports our conclusion on the existence of threshold charge density (or electrode potential) values illustrated in Fig. 3. Of course, a small size of the model system and relatively short simulation time bring in uncertainties into the computed critical values. We believe, however, that our conclusions are true at least at a semi-quantitative level.

The PMF for the intrusion of a single  $[\text{BMIM}]^+$  cation demonstrates significantly different shape (Fig. 6b, PMF2) as compared with that for the anion. A deep minimum at the distance  $z = 7$  Å appears in the calculated energy profile which originates from a competition of three different types of interactions: metal-ion, thiol-thiol and ion-thiol. This minimum, however, almost disappears when the desolvation contribution is included (red curve PMF1 in Fig. 6b).

The PMF profile was found to be steeper for the anion which is in agreement with its lower critical cathodic potential value (Fig. 3). As the cavity formation energy contributes significantly to the overall energy barrier for penetration, the presence of various types of defects is likely to lower the free energy of the ion at the surface thus enhancing the permeability of the monolayer. Thus, our findings reinforce the hypothesis about the important role of defects in real alkanethiol SAMs.

Using IR spectroscopy the authors of ref 14 showed that the permeation of ions into the monolayer of thiols causes significant structural changes (decreasing the tilt angle and the destruction of a crystalline-like structure of the SAM). Our results support such conclusions. The permeation of cations into the monolayer causes changes in the alkyl chain conformations and tilt angle which induces a local disordering of the monolayer structure (Fig. S4, ESI<sup>†</sup>). The permeation of

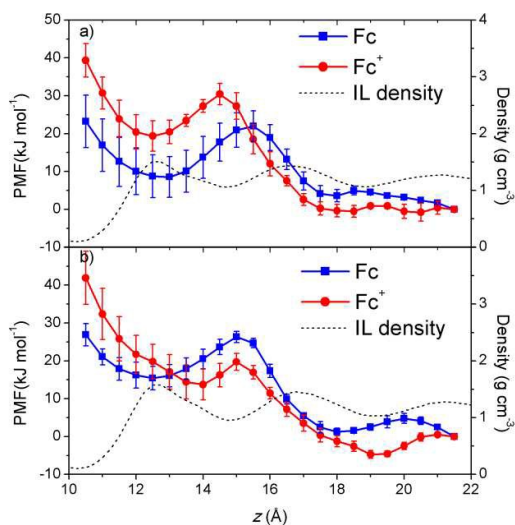


**Fig. 7** PMF profiles for Fc and Fc<sup>+</sup> at the Au(111)/SC<sub>6</sub>H<sub>13</sub>/[bmim][BF<sub>4</sub>] interface for the cases of uncharged (a) and charged (b) electrode surfaces ( $\sigma = 15 \mu\text{C}\cdot\text{cm}^{-2}$ ).

smaller anions results in noticeable structural changes only in the vicinity of gold surface.

In the next Section we extend our analysis to a redox-active solute at the Au(111)/SAM/IL interface.

### 3.4. Redox couple Fc/Fc<sup>+</sup> at the alkanethiol/[bmim][BF<sub>4</sub>] interface

The main issue which will be in focus now is whether short-chain alkanethiol monolayers can be employed in electrochemical kinetic studies, similar to those performed in refs 1-4 and 11. This problem is important indeed because the permeation of reactants inside the monolayers in ET studies at metal/alkanethiol/IL interfaces would affect significantly the measured rate constant values.

A Fc<sup>+</sup>/Fc redox couple was employed as a model probe in our previous study<sup>11</sup> and its formal potential is located in the region of increased capacitance. We performed MD simulations of the Au(111)/alkanethiol/IL/Fc<sup>0/+</sup> interface in order to elucidate whether the reactant (product) can penetrate into the monolayer and approach the electrode surface. If the ferrocene (ferrocenium) permeation would really take place, the experimental rate constant dependence would hardly be informative. Due to drastically reducing the electrode-reactant separation.

In a conventional electrochemical kinetic experiment the reactant concentration is quite low (0.5-5 mM in aqueous solutions and 5-15 mM in ILs). That is why it is troublesome to simulate a system with a realistic reactant concentration, as the MD cell would contain only 5-6 Fc/Fc<sup>+</sup> molecules. To avoid this problem, we constructed the PMF profiles for Fc and Fc<sup>+</sup> at the SC<sub>6</sub>H<sub>13</sub>/[bmim][BF<sub>4</sub>] interface (Fig. 7). The PMF, i.e. the reactant (product) free energy vs. distance plays an exceedingly important role in molecular modeling interfacial ET processes.<sup>29</sup> This quantity provides estimations of work terms and the distances of closest approach. The latter governs in turn the ET regime (adiabatic or diabatic).

Fig. 7a show the potentials of mean force for Fc and Fc<sup>+</sup> near the uncharged surface ( $\sigma = 0$ ). It can be argued from comparison of the PMF and IL mass density profiles that a considerable solvent structuring near the interface influences the distribution of reactant molecules. At the distance from the Au surface  $z = 12.5 \text{ \AA}$  the PMF profile reveals an energy minimum, which results in an increased reactant concentration in this region. At  $z < 12.5 \text{ \AA}$  the PMF profile demonstrates a steep rise caused by the van der Waals repulsive forces. As we demonstrated in previous sections, a channel of the appropriate size should be formed to facilitate the ion penetration into the monolayer. As the cross section area of the Fc molecule is larger than the size of IL cation, the barrier for the Fc permeation has to be significantly higher. The permeation of only the IL ions (not the reactant species) can be expected, therefore for the charged electrode surface.

The energy minimum at  $z = 12.5 \text{ \AA}$  is separated from bulk IL by an energy barrier, which is higher for Fc<sup>+</sup> than for Fc. This is in agreement with our previous MD simulations of Au(111)/[bmim][BF<sub>4</sub>] interface.<sup>29</sup> This difference originates most likely from the higher desolvation energy for charged species than that for neutral one.

At positively charged Au(111) ( $\sigma = 15 \mu\text{C}\cdot\text{cm}^{-2}$ ) the PMF profiles exhibits no significant changes. For Fc<sup>+</sup> ion the free energy minimum is shifted towards longer distances from the metal surface and the potential rise is sharper in the vicinity of the monolayer, which is the result of stronger electrostatic repulsion between the Fc<sup>+</sup> cation and the positively charged surface. Again, the free energy profiles exhibited in Fig. 7 look qualitatively very similar to those obtained earlier for the Au/IL interface.<sup>29</sup>

Although we did not calculate the PMF for Fc and Fc<sup>+</sup> for shorter electrode - reactant distances, one can argue that in contrast to the IL anions and cations the permeation of a Fc<sup>+</sup>/Fc couple inside the monolayer (even having defects) at the positively charged surface is energetically unfavorable. Firstly, it follows from the PMF shape shown in Fig. 7 that only a very low concentration of the Fc and Fc<sup>+</sup> solutes can be found in the immediate vicinity of the SAM/IL interface. Secondly, as the effective size of ferrocene and ferrocenium molecules is larger in comparison with the IL components, more energy is needed to change the local structure of the monolayer. Thirdly, at experimental conditions the Au(111) electrode surface is positively charged which also decreases the penetration probability of Fc<sup>+</sup>. Therefore, previous kinetic studies of the ET in this system at short-chain alkanethiol-modified gold should be regarded as reliable.

## 4. Conclusions

We have investigated the permeability of alkanethiol defectless monolayers with  $(\sqrt{3} \times \sqrt{3})_{R30^\circ}$  structure in [bmim][BF<sub>4</sub>] IL at neutral and charged Au(111) electrode surface. After a threshold value of external electric field is attained, the IL ions were found to penetrate through the close-packed monolayer even in the absence of defective sites. The mechanism of IL ions permeation involves the transport of

individual IL ions into the monolayer, in contrast to aqueous systems where a polar channel of water molecules is formed prior to the permeation.

The free energy profiles describing the penetration of IL ions through the defectless monolayer show significant energy barriers resulting from desolvation and the cavity formation.

For the monolayers with different alkanethiol chain lengths critical surface charge density values range between  $\sim 5 \div 10 \mu\text{C}\cdot\text{cm}^{-2}$  which lie beyond the monolayer stability region. This might be regarded as some manifestation of the presence of the SAM defects at real electrochemical interfaces lowering the energy barrier for ion permeation. Thus, monolayers with ideal packing are most likely impermeable towards the IL ions at electrode charge densities realized in experiment.

In spite of a rather pronounced permeation of the IL ions inside the SAM starting from a threshold value of the electrode charge, neither  $\text{Fc}^+$  nor  $\text{Fc}$  penetrates through the monolayer. The potentials of mean forces calculated for ferrocene and ferrocenium at the SAM/IL interface resemble those obtained previously for the same species at the Au(111)/IL interface and predict a significantly low concentration of the both species at the SAM "surface". A further transport of  $\text{Fc}^+$  and  $\text{Fc}$  looks hardly feasible because of some additional reasons as well (the large reactant size and positive electrode charge densities occurring in experiment). It is important to note that the penetration of the IL components through the SAM does not change practically its thickness. We argue, therefore that kinetic studies of ET ( $\text{Fc}/\text{Fc}^+$ ) through alkanethiol monolayers with variable thickness can be performed in ILs as well, despite permeating properties of real defective SAMs.

## Acknowledgements

This work was supported in part by the Russian Foundation for Basic Research (projects No. 12-03-31748mol\_a, 14-03-00935a). We are deeply indebted to G.A. Tsirlina for useful discussions and valuable comments. The computational resources of the Joint Supercomputer Center of RAS and Supercomputing Center of Lomonosov Moscow State University are highly appreciated. Kislenko S.A. acknowledges a scholarship awarded by the Zamaraev International Charitable Scientific Foundation.

## Notes and references

- 1 A. M. Becka and C. J. Miller, *J. Phys. Chem.*, 1992, **96**, 2657–2668.
- 2 A. M. Becka and C. J. Miller, *J. Phys. Chem.*, 1993, **97**, 6233–6239.
- 3 C. Miller, P. Cuendet and M. Gratzel, *J. Phys. Chem.*, 1991, **95**, 877–886.
- 4 L. V. Protsailo and W. R. Fawcett, *Electrochimica Acta*, 2000, **45**, 3497–3505.
- 5 J. J. Gooding, F. Mearns, W. Yang and J. Liu, *Electroanalysis*, 2003, **15**, 81–96.
- 6 L. Newton, T. Slater, N. Clark and A. Vijayaraghavan, *J. Mater. Chem. C*, 2013, **1**, 376–393.
- 7 A. M. Kuznetsov and J. Ulstrup, *Electron Transfer in Chemistry and Biology*; Wiley: Chichester, U.K., 1999.

- 8 M. D. Porter, T. B. Bright, D. L. Allara and C. E. D. Chidsey, *J. Am. Chem. Soc.*, 1987, **109**, 3559–3568.
- 9 J. Dai, Z. Li, J. Jin, Y. Shi, J. Cheng, J. Kong and S. Bi, *Biosens. Bioelectron.*, 2009, **24**, 1074–1082.
- 10 E. Boubour and R. B. Lennox, *J. Phys. Chem. B*, 2000, **104**, 9004–9010.
- 11 V. A. Nikitina, A. V. Rudnev, G. A. Tsirlina and T. Wandlowski, *J. Phys. Chem. C*, 2014, **118**, 15970–15977.
- 12 E. Boubour and R. B. Lennox, *Langmuir*, 2000, **16**, 7464–7470.
- 13 B. O'Brien, H. Sahalov and P. C. Searson, *Appl. Phys. Lett.*, 2010, **97**, 043110–043112.
- 14 N. Darwish, P. K. Eggers, S. Ciampi, Y. Zhang, Y. Tong, S. Ye, M. N. Paddon-Row and J. J. Gooding, *Electrochem. Commun.*, 2011, **13**, 387–390.
- 15 C. Gupta, M. A. Shannon and P. J. A. Kenis, *J. Phys. Chem. C*, 2009, **113**, 9375–9391.
- 16 C. Gupta, M. A. Shannon and P. J. A. Kenis, *J. Phys. Chem. C*, 2009, **113**, 4687–4705.
- 17 H. Sahalov, B. O'Brien, K. J. Stebe, K. Hristova and P. C. Searson, *Langmuir*, 2007, **23**, 9681–9685.
- 18 T. D. Dolidze, D. E. Khoshtariya, P. Illner and R. V. Eldik, *Chem. Commun.*, 2008, 2112–2114.
- 19 D. E. Khoshtariya, T. D. Dolidze and R. V. Eldik, *Chem. Eur. J.*, 2009, **15**, 5254–5262.
- 20 D. Wei, A. Ivaska, *Anal. Chim. Acta*, 2008, **607**, 126–135.
- 21 R. P. Janek, W. R. Fawcett and A. Ulman, *J. Phys. Chem. B*, 1997, **101**, 8550–8558.
- 22 E. Boubour and R. B. Lennox, *Langmuir*, 2000, **16**, 4222–4228.
- 23 S. A. Kislenko, V. A. Nikitina and R. R. Nazmutdinov, *High Energy Chemistry*, 2015, **49**, 341–346.
- 24 C. Vericat, M. E. Vela, G. Benitez, P. Carro and R. C. Salvarezza, *Chem. Soc. Rev.*, 2010, **39**, 1805–1834.
- 25 K. Slowinski, R. V. Chamberlain, C. J. Miller and M. Majda, *J. Am. Chem. Soc.*, 1997, **119**, 11910–11919.
- 26 B. Rai, P. Sathish, C. P. Malhotra and K. G. Ayappa, *Langmuir*, 2004, **20**, 3138–3144.
- 27 J. N. C. Lopes, J. Deschamps and A. A. H. Padua, *J. Phys. Chem. B*, 2004, **108**, 2038–2047.
- 28 J. N. C. Lopes, P. Cabral do Couto and M. E. Minas da Piedade, *J. Phys. Chem. A*, 2006, **110**, 13850–13856.
- 29 V. A. Nikitina, S. A. Kislenko, R. R. Nazmutdinov, M. D. Bronshtein and G. A. Tsirlina, *J. Phys. Chem. C*, 2014, **118**, 6151–6164.
- 30 I.-C. Yeh and M. L. Berkowitz, *J. Chem. Phys.*, 1999, **111**, 3155–3162.
- 31 W. Smith, T. R. Forester and I. T. Todorov, The DL\_POLY Classic User Manual, D. L., UK. The DLPOLY website is [http://www.ccp5.ac.uk/DL\\_POLY\\_CLASSIC/](http://www.ccp5.ac.uk/DL_POLY_CLASSIC/).
- 32 S. A. Kislenko, R. H. Amirov and I. S. Samoylov, *Phys. Chem. Chem. Phys.*, 2009, **11**, 5584–5590.
- 33 S. A. Kislenko, R. H. Amirov and I. S. Samoylov, *J. Phys.: Conf. Ser.*, 2013, **418**, 012021–012028.
- 34 S. A. Kislenko, R. H. Amirov and I. S. Samoylov, *J. Phys. Chem. C*, 2013, **117**, 10589–10596.
- 35 K. Kinoshita and T. Y. Tsong, *Biochim. Biophys. Acta*, 1979, **554**, 479–497.
- 36 G. C. Troiano, L. Tung, V. Sharma and K. J. Stebe, *Biophys. J.*, 1998, **75**, 880–888.
- 37 R. A. Bockmann, B. L. Groot, S. Kakorin, E. Neumann and H. Grubmuller, *Biophys. J.*, 2008, **95**, 1837–1850.
- 38 M. D. Levi, N. Levy, S. Sigalov, G. Salitra, D. Aurbach and J. Maier, *J. Am. Chem. Soc.*, 2010, **132**, 13220–13222.
- 39 Y. Shilina, M. D. Levi, V. Dargel, D. Aurbach, S. Zavorine, D. Nucciarone, M. Humeniuk and I. C. Halalay, *J. Electrochem. Soc.*, 2013, **160**, A629–A635.